Lyapunov Designed Super-Twisting Sliding Mode Control for Wind Energy Conversion Optimization

C. Evangelista*†, P. Puleston*, F. Valenciaga* and L. Fridman**

***Abstract*— This work explores an adaptive second order sliding mode control strategy to maximize the energy production of a wind energy conversion system (WECS) simultaneously reducing the mechanical stress on the shaft. Such strategy successfully deals with the random nature of wind speed, the intrinsic nonlinear behavior of the WECS and the presence of model uncertainties and external perturbations acting on the system.**
The synthesized adaptive controller is designed from a modified version of the super-twisting (ST) algorithm with variable gains. The suitability of the proposed strategy is proved by extensive computer aided simulations employing a comprehensive model of the system emulating realistic conditions of operation, i.e., considering variations in the parameters and including external disturbances.
Additionally, a second controller based on the traditional ST algorithm is also designed and simulated. Results are presented and discussed, in order to establish a comparison framework.

***Index Terms*— Sliding Mode Control, Wind Power Generation, Super-Twisting.**

I. INTRODUCTION

It is well known that due to several reasons, worldwide attention has turned to renewable energy sources, among which wind represents one of the most interesting options. Its exploitation has been one of the most dynamically growing for the last years. By the end of 2010, wind turbines were generating 2.5% of the world electricity consumption and the global wind installed capacity exceeded 197GW [1], [2].

This growing trend must be accompanied by continuous technological development and optimization, leading to better options concerning reductions in costs, integration to the grid and improvements regarding turbine performance and reliability in the electricity delivery. Among the main research subjects in the wind energy field there is the exploration of novel control strategies, which must cope with the exacting characteristics presented by WECS such as the nonlinear behavior of the system, usual uncertainties in both the aerodynamic and the electrical models and the presence of external perturbations, and the random variability of the wind.

In this context, it results of interest to explore the use of second order sliding mode (SOSM) algorithms, which are an excellent option to control nonlinear uncertain systems operating in perturbed environments [3]. Roughly speaking, SOSM techniques consist of zeroing the sliding variable σ and its first time derivative $\dot{\sigma}$ in finite time, through a continuous control $u(t)$ acting discontinuously on its second time derivative, $\ddot{\sigma}$, reducing strongly the chattering phenomenon. They result in controllers with several attractive characteristics [4]-[16]:

- Robustness with respect to various internal and external disturbances and model uncertainties, allowing accurate regulation and tracking.
- Finite-time convergence.
- Reduction of mechanical stresses and chattering (i.e., high-frequency vibrations of the controlled system), compared to standard sliding mode strategies, given that the applied control actions are continuous.
- Relatively simple control laws, which entails low real time computational burden.
- The design procedure is capable of dealing with nonlinear descriptions of the system, therefore wider ranges of operation are attained, in comparison to design techniques based on model linearization.

This work presents a controller based on the ST algorithm with variable gains proposed by Dávila, Moreno and Fridman [17], using Lyapunov techniques. In particular, it has been applied and developed to control a grid-connected variable-speed WECS topology with slip power recovery, which can be electronically controlled. Its variable speed feature allows to seek power conversion maximization in the zone of operation known as partial load zone, where the wind speed is below the rated of the turbine. The followed control objective was to optimize its power conversion efficiency, reducing mechanical fatigue and attenuating the output chattering.

Additionally, a non adaptive SOSM controller is designed, in order to both assess its applicability to the studied WECS and to compare its performance with the adaptive-gain proposal. Suitable candidates could be a classic ST structure or other constant-gain SOSM algorithms (e.g. Twisting or Sub-optimal) with the incorporation of an integrator to increase the relative degree. The ST algorithm, originally presented by Levant [11], has been preferred given that it can be directly applied to systems of relative degree 1 (as the considered WECS) and besides, it does not require information of $\dot{\sigma}$ for its implementation. For comparative reasons, the fixed-gain ST controller has been tuned following the development presented by Moreno and Osorio [18], since the design method is based on Lyapunov and is analogous to the one proposed for the variable-gain ST algorithm.

The paper is organized as follows. The WECS and the control objective are briefly explained in Section II. The control design is described in Section III, including the development of the variable-gain and of the fixed-gain ST controllers, in III-A and III-B respectively. Simulation results are shown in Section IV, where the two strategies are evaluated. Finally, conclusions are presented in Section V.

*CONICET and LEICI, Facultad de Ingeniería, UNLP, Argentina.
†cae@ing.unlp.edu.ar
** Departamento de Ingeniería de Control y Robótica, División de Ingeniería Eléctrica, Facultad de Ingeniería, UNAM, México.

II. WECS DESCRIPTION

Grid-connected WECS based on a double-output induction generator (DOIG) with slip power recovery are considered. Such variable-speed configuration can operate at different speeds but generates electricity at the constant frequency and voltage fixed by the grid and, adequately controlled, allows power conversion maximization and mechanical stress alleviation. Particularly in this paper, a simple topology has been selected as a case of study, namely one that uses a static Kramer drive (SKD) as slip power recovery drive. A schematic diagram of this configuration is shown in Fig. 1.

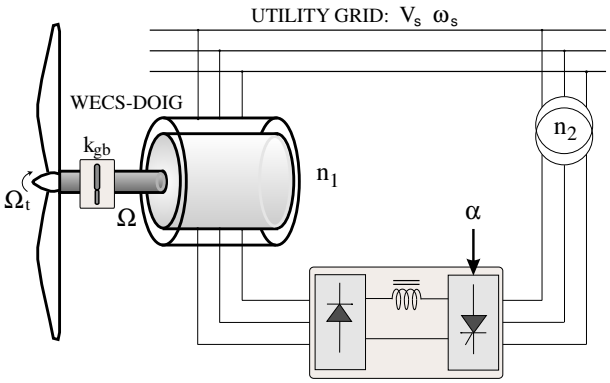

Fig. 1. WECS-DOIG with static Kramer drive.

As it can be observed, both stator and rotor circuits provide power to the grid, making the system capable of generation above its rated power. While the former is directly delivered to the grid, the latter is partially recovered through an electronic converter, which processes only the recovered power. This converter consists of an uncontrolled bridge rectifier, a smoothing reactor and a line commutated inverter, whose firing angle α can be modified to control the generator torque, and hence the system operation speed and the operation point [19], [20], [21].

Starting the description of the WECS with the aerodynamic subsystem, it should be mentioned that the present work focuses on the partial load zone of operation, within which the control objective is to extract the maximum power from the wind. As it can be seen in Fig. 2, the partial load zone is the operation zone between the cut-in (when the wind energy is not sufficient to move on the turbine) and the rated wind speed [22]. Operation above the rated wind speed is not considered here and the existence of a power limiting mechanism has been assumed (possibly by actively or passively changing its aerodynamic characteristics).

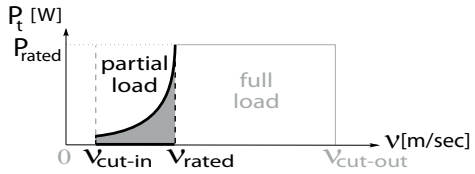

Fig. 2. Wind turbine operation zone.

For the subsequent analysis a rigid drive train has been assumed and for mathematical simplicity every turbine variable in the paper has been rendered at the fast shaft or generator side through the transmission ratio k_{gb} of the gear box (see Appendix *A*).

The mechanical power a real turbine can capture is only a fraction of the available power in the wind and it can be written as [23]:

$$P_t = 0.5\pi\rho R^2 C_p(\lambda)\nu^3 \tag{1}$$

where ν is the wind speed, ρ the air density, R the blades length and $C_p(\lambda)$ the conversion efficiency or power coefficient of the WECS. This coefficient is a nonlinear function of the called tip speed ratio $\lambda = R\Omega/\nu$, with Ω the mechanical rotation speed, and depends on the shape and geometrical dimensions of the rotor, presenting for a turbine with fixed pitch a single maximum.

Therefore, power efficiency maximization is obtained if the tip speed ratio is kept equal to λ_{opt}, which can be accomplished by controlling the system speed operation to track the variable optimum reference given by [22], [23]:

$$\Omega_{ref} = \frac{\lambda_{opt}\nu}{R} \tag{2}$$

The power coefficient curve for the three-bladed turbine used in this work, modeled as $C_p(\lambda) = \sum_{i=0}^{3} c_i\lambda^i$, is depicted in Fig. 3.

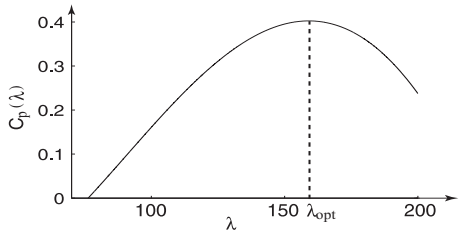

Fig. 3. Power coefficient versus tip speed ratio.

An expression for the turbine torque T_t is obtained from the quotient P_t/Ω and, defining the torque coefficient of the turbine as $C_t(\lambda) = C_p(\lambda)/\lambda$, it can be written as:

$$T_t = 0.5\pi\rho R^3 C_t(\lambda)\nu^2 \tag{3}$$

Regarding the electromechanical subsystem of the WECS, it is reasonable to assume that the electrical dynamics are considerably faster than the mechanical ones. Therefore, a reduced order model considering the dominant dynamics is used in this work for the controller design. Then, the nonlinear dynamic equation of the system can be straightforwardly obtained by applying Newton's second law, including a term $\mathrm{g}(\cdot)$ to consider friction, uncertainties and other disturbances, it can be stated as:

$$\dot{\Omega} = \frac{1}{J}\Big(T_t(\Omega,\nu(t)) + T_e(\Omega,u)\Big) + \mathrm{g}(\Omega,t) \tag{4}$$

where J is the inertia of the combined rotating parts, T_e is the electrical resistant torque of the generator ($T_e < 0$ as generator), and u is the control action. Although the generator torque is physically modified by the controlled firing angle

α, in this design framework the variable $u = |\cos(\alpha)|$ is used as the control action for simplicity's sake. In this context, the expression of the generator torque is given by [24]:

$$T_e(\Omega, u, t) = \frac{3V_s'^2 s R_{eq}}{\Omega_s\left[(sR_s' + R_{eq})^2 + (s\omega_s L)^2\right]} \tag{5}$$

where

$$R_{eq} = \frac{s}{s^2 - n^2u^2}\Big[sR_b + n^2u^2R_s' - nu\sqrt{\left|(R_b + sR_s')^2 + \omega_s^2L^2\left(s^2 - n^2u^2\right)\right|}\Big]$$

and $R_b = R_r + 0.55R_f$, $L = L_s' + L_r$. R_s, R_r and R_f are the resistance of stator, rotor and dc-link, respectively, L_s and L_r are the leakage inductances of stator and rotor windings, Ω_s and ω_s are the mechanical and electrical synchronous speeds, $s = 1 - \Omega/\Omega_s$ is the generator slip, V_s the stator voltage, and $n = \frac{n_1}{n_2}$, with n_1 and n_2 the turns ratios of the generator and the step-down transformer respectively. Note that a single quotation mark applied to a stator variable indicates that it has been referred to the rotor windings by n_1.

The torque characteristics T_t and $-T_e$ are schematically depicted in Fig. 4, in the $T - \Omega$ plane. The curves in solid lines show the variation of $-T_e$ with Ω for some values of the control action u, while the variation of T_t is depicted in dotted lines for several wind speeds. The geometric locus corresponding to the points of maximum power generation is also presented in the picture in bold dashed line.

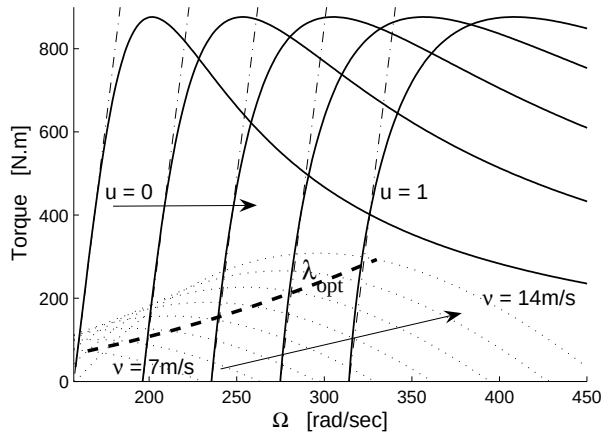

Fig. 4. Torque versus rotational speed characteristics of the DOIG (solid lines). Wind turbine characteristic for different wind speeds (dotted lines). Affine approximation to DOIG characteristic (dash-dotted lines). Maximum power generation locus (bold dashed line).

III. CONTROLLER DESIGN

The expression of the generator torque can be rewritten as:

$$\begin{aligned} T_e(\Omega, u, t) &= \frac{3V_s'^2 n}{\Omega_s R_b}u + \frac{3V_s'^2}{\Omega_s R_b}\Big(1 - \frac{\Omega}{\Omega_s}\Big) + \Delta T_e(\Omega, t) \\ &= B_1 u + T_{e_1}(\Omega) + \Delta T_e(\Omega, t) \end{aligned} \tag{6}$$

where the two first terms correspond to an affine in the control approximation of the generator torque and the third term, ΔT_e, takes into account the remaining differences.

In the zone of operation, where the torque keeps below the rated, the term $\Delta T_e(\cdot)$ is considerably small and, consequently, the affine description results a good approximation for T_e (see characteristic in dash-dotted lines in Fig. 4).

Replacing (6) into (4), it results in:

$$\dot{\Omega} = \frac{B_1}{J}u + \frac{T_t(\Omega, \nu) + T_{e_1}(\Omega)}{J} + \mathrm{g}(\Omega, t) + \frac{\Delta T_e(\Omega, t)}{J} \tag{7}$$

At this point, to accomplish the speed reference tracking the sliding variable is chosen as

$$\sigma = \frac{J}{B_1}\big(\Omega - \Omega_{ref}(t)\big) \tag{8}$$

In this way, the 2-sliding condition $\dot{\sigma} = \sigma = 0$ guarantees the main control objective $\Omega = \Omega_{ref}$. At the same time, the inclusion of the constant factor J/B_1 allows to express the sliding dynamics in the regular form using (2), (7) and (8):

$$\dot{\sigma} = \frac{J}{B_1}\dot{\Omega} - \frac{J\lambda_{opt}}{B_1 R}\dot{\nu} \;=\; u + F(\sigma, t) + G(\sigma, t) \tag{9}$$

$$F(\sigma, t) = \frac{1}{B_1}\Big(T_t(\Omega, \nu) + T_{e_1}(\Omega) - \frac{J\lambda_{opt}}{R}\dot{\nu}\Big) \tag{10}$$

$$G(\sigma, t) = \frac{1}{B_1}\Big(\mathrm{g}(\Omega, t) + \Delta T_e(\Omega, t) + J\,\Delta\Omega_{ref}(t)\Big) \tag{11}$$

where $\Omega = \frac{B_1}{J}\sigma + \frac{\lambda_{opt}}{R}\nu$ and $\Delta\Omega_{ref}(t)$ considers the errors in the determination of the reference. Function F represents the nominal or undisturbed design model and function G takes into account measurement and modeling errors, uncertainties in the parameters and external disturbances.

A two-component control action is proposed as $u = u_{eq} + \tilde{u}$, where u_{eq} is the equivalent control for system (7) and $\tilde{u}$ is designed using a modified version of the ST algorithm.

The expression of u_{eq} is computed from the undisturbed system (9) (i.e. $G(\sigma, t) = 0$). It is obtained solving for u the algebraic equation $\dot{\sigma} = 0$, on the sliding surface (i.e. with $\sigma = 0$) [25]. Writing $k_o = \frac{\lambda_{opt}}{R}$, the expression for u_{eq} is:

$$u_{eq} = -F(0, t) \;=\; \frac{Jk_o\dot{\nu} - T_t(k_o\nu, \nu) - T_{e_1}(k_o\nu)}{B_1} \tag{12}$$

Using this formula, (9) can be written as:

$$\dot{\sigma} = u_{eq} + \tilde{u} + F(\sigma, t) + G(\sigma, t) = \tilde{u} + \tilde{G}(\sigma, t) \tag{13}$$

where $\tilde{G}(\sigma, t) = F(\sigma, t) - F(0, t) + G(\sigma, t)$. This function can be divided into two terms such as $\tilde{G}(\sigma, t) = \tilde{G}_1(\sigma, t) + \tilde{G}_2(t)$:

$$\tilde{G}_2(t) = \tilde{G}(0, t) \tag{14}$$

$$\tilde{G}_1(\sigma, t) = \tilde{G}(\sigma, t) - \tilde{G}(0, t) \tag{15}$$

The design of $\tilde{u}$ is based on certain bounding functions which must be found for $\tilde{G}_1(\sigma, t)$ and the time derivative of $\tilde{G}_2(t)$.

In the following subsections, two designs are developed for this term. In the main proposal, $\tilde{u}$ has variable gains and is a variation of the Lyapunov based design presented in [17]. Its adaptive characteristic is intended to be beneficial regarding output chattering and mechanical efforts applied to the shaft. As a second case of study, the Lyapunov based standard ST algorithm proposed in [18] is applied to this control problem.

A. Variable-gain Super-Twisting

The variable-gain ST control action term $\tilde{u}$ has the form:

$$\tilde{u} = -k_1(\sigma,t)\phi_1(\sigma) - \int_0^t k_2(\sigma,\tau)\phi_2(\sigma)d\tau \tag{16}$$

$$\phi_1(\sigma) = k_c|\sigma|^{\frac{1}{2}}\text{sign}(\sigma), \qquad k_c > 0 \tag{17}$$

$$\phi_2(\sigma) = \phi_1^{'}(\sigma)\phi_1(\sigma) = \frac{k_c^2}{2}\text{sign}(\sigma) \tag{18}$$

The constant k_c is not present in the original algorithm. It has been considered here as an additional tuning parameter, to allow a better behaviour of the controlled system with respect to chattering. Then, defining $z_1 = \sigma$ and $z_2 = -\int_0^t k_2(\sigma,t)\phi_2(\sigma)dt + \tilde{G}_2(t)$ as the new states, the closed loop system dynamics for (13) with the variable-gain ST control law given in (16) can be written as

$$\begin{cases} \dot{z_1} &= -k_1(z_1,t)\phi_1(z_1) + z_2 + \tilde{G}_1(z_1,t) \\ \dot{z_2} &= -k_2(z_1,t)\phi_2(z_1) + \dfrac{d}{dt}\tilde{G}_2(t) \end{cases} \tag{19}$$

A Lyapunov function can be found for this system so that, if the components of $\tilde{G}$ can be bounded such that:

$$|\tilde{G}_1(z_1,t)| \leq \varrho_1(z_1,t)|\phi_1(z_1)| = \varrho_1(z_1,t)\, k_c\, |z_1|^{\frac{1}{2}} \tag{20}$$

$$|\frac{d}{dt}\tilde{G}_2(t)| \leq \varrho_2(z_1,t)|\phi_2(z_1)| = \varrho_2(z_1,t)\, \frac{k_c^2}{2} \tag{21}$$

with some known positive functions $\varrho_1(z_1,t)$ and $\varrho_2(z_1,t)$, and for four constants $\epsilon > 0$, $p_1 > 0$, $p_2 < -\epsilon$ and $p_3 > 0$ verifying $p_1 p_3 > p_2^2$, the varying gains of $\tilde{u}$ are selected as:

$$k_1(z_1,t) = \frac{p_3}{p_1 p_3 - p_2^2}\left(\frac{(p_3\varrho_2 - p_2\varrho_1)^2}{-4(p_2+\epsilon)} + p_1\varrho_1 - \right.$$
$$\left. - p_2\varrho_2 - \frac{p_1 p_2}{p_3} + \epsilon\right) + \delta\,, \qquad \delta > 0 \tag{22}$$

$$k_2(z_1,t) = \frac{p_1}{p_3} - \frac{p_2}{p_3}k_1(z_1,t)\,, \tag{23}$$

with δ small, then the trajectories of the controlled system (19) converge to the origin in finite time despite the perturbations.

This can be proved using the following Lyapunov function:

$$V(z) = \zeta^T P \zeta \tag{24}$$

with $\zeta^T = [\phi_1(z_1),\ z_2] = [k_c|z_1|^{1/2}\text{sign}(z_1),\ z_2]$ and

$$P = \begin{bmatrix} p_1 & p_2 \\ p_2 & p_3 \end{bmatrix} = P^T > 0$$

Then, a procedure similar to the one developed in the general proof in [17] is followed. Given that conditions (20)-(23) are verified for the WECS under study, it can be shown that the time derivative of the Lyapunov function is bounded by:

$$\dot{V} \leq -\epsilon\phi_1^{'}(z_1)\zeta^T\zeta = -\frac{\epsilon k_c}{2|z_1|^{1/2}}\|\zeta\|_2^2 \tag{25}$$

where $\|\zeta\|_2^2 = k_c^2|z_1| + z_2^2$ is the Euclidean norm. Hence, from the standard inequality for quadratic forms:

$$\lambda_{Pm}\|\zeta\|_2^2 \leq \zeta^T P\zeta = V(z) \leq \lambda_{PM}\|\zeta\|_2^2 \tag{26}$$

where λ_{Pm} and λ_{PM} are the minimum and the maximum eigenvalues of P, it stands that:

$$V^{\frac{1}{2}} \geq \lambda_{Pm}^{\frac{1}{2}}\|\zeta\|_2 \geq \lambda_{Pm}^{\frac{1}{2}}k_c|z_1|^{\frac{1}{2}} \tag{27}$$

And finally, from (25), (26) and (27):

$$\dot{V} \leq -\frac{\epsilon k_c}{2|z_1|^{\frac{1}{2}}}\frac{V}{\lambda_{PM}} \leq -\frac{\epsilon k_c^2\lambda_{Pm}^{\frac{1}{2}}}{2\lambda_{PM}}V^{\frac{1}{2}} = -\gamma V^{\frac{1}{2}} \tag{28}$$

with $\gamma = \frac{\epsilon k_c^2\lambda_{Pm}^{\frac{1}{2}}}{2\lambda_{PM}} > 0$, which shows that $V(z)$ is a strong Lyapunov function. Consequently, by the comparison principle [26], $V(z)$ and, therefore, the trajectories of (19) converge to zero in finite time.

The expression of $\tilde{G}(z_1,t)$ for the WECS under study is given in Appendix *B*. It has been computed by propagation of error of (9), considering uncertainties in nominal parameters, variable measurement errors and the addition of disturbances. In this case of study, the parameters taken into account as sources of errors and perturbations were the electrical resistances ($\pm 20\%$ of their nominal values), the grid nominal voltage ($\pm 15\%$ of its nominal value), bounded wind speed measurement errors and the coefficients of the polynomial which describes the torque coefficient of the turbine C_t ($\pm 10\%$ of their nominal values). As a strong disturbance, an unmodeled friction torque has been included, computed as a quadratic function of the rotational speed with the addition of a random varying independent term (up to $\pm 10\%$ of the friction), generated as band-limited white noise.

Following the described procedure, analytical expressions have been found for the bounding functions:

$$\varrho_1(z_1,t) = \frac{1}{k_c}|z_1|^{\frac{1}{2}}(A_1 + A_2\,|z_1| + A_3\,z_1^2) \tag{29}$$

$$\varrho_2(z_1,t) = \frac{A_0}{k_c^2} \tag{30}$$

where the values for constants A_0-A_3 are given in Appendix *A*. The final tuning was aided by simulation tests, selecting the values for the remaining control design parameters according to the objective of reducing mechanical loads and output chattering in the controlled system. The chosen values for k_c, p_1, p_2, p_3, ϵ and δ, to compute $k_1(z_1,t)$ and $k_2(z_1,t)$ according to (22)-(23) are also in Appendix *A*.

B. Fixed-gain Super-Twisting

In this case, the control action expression for the term $\tilde{u}$ in (13) is similar to (16), but using fixed gains:

$$\tilde{u} = -k_1\phi_1(\sigma) - k_2\int_0^t \phi_2(\sigma)d\tau \tag{31}$$

where $\phi_1(\sigma)$ and $\phi_2(\sigma)$ are the ones in (17)-(18) with $k_c = 1$:

$$\phi_1(\sigma) = |\sigma|^{\frac{1}{2}}\text{sign}(\sigma) \tag{32}$$

$$\phi_2(\sigma) = \phi_1^{'}(\sigma)\phi_1(\sigma) = \frac{1}{2}\text{sign}(\sigma) \tag{33}$$

Proceeding similarly to the variable-gain case, new states $z_1 = \sigma$ and $z_2 = -k_2 \int_0^t \phi_2(\sigma)dt + \tilde{G}_2(t)$ are defined. Then, bounding the components of $\tilde{G}$ as

$$|\tilde{G}_1(z_1,t)| \leq \delta_1 \, |\phi_1(z_1)| \, = \delta_1 \, |z_1|^{\frac{1}{2}} \tag{34}$$

$$|\frac{d}{dt}\tilde{G}_2(t)| \leq \delta_2 \tag{35}$$

with δ_1 and δ_2 positive constants, the proposed Lyapunov function (24) guarantees the trajectories of the controlled WECS converge to the origin in finite time, having chosen the fixed gains to verify [18]:

$$k_1 > 2\delta_1 \tag{36}$$

$$k_2 > k_1 \frac{5\delta_1 + 6\delta_2 + 4(\delta_1 + \delta_2/k_1)^2}{2(k_1 - 2\delta_1)} \tag{37}$$

It follows from (20)-(21) and (34)-(35) that δ_1 and δ_2 for the WECS under study can be obtained bounding the functions $\varrho_1(z_1,t)$ and $\varrho_2(z_1,t)$ in (29)-(30), found for the calculation of the variable gains. The constants δ_1 and δ_2 must satisfy:

$$\delta_1 \geq |z_1|^{\frac{1}{2}}(A_1 + A_2 \, |z_1| + A_3 \, z_1^2) \tag{38}$$

$$\delta_2 \geq \frac{A_0}{2} \tag{39}$$

Clearly, a global use of this algorithm would not be convenient. Therefore, it is necessary to establish a maximum for $z_1 = \sigma = \frac{J}{B_1}(\Omega - \Omega_{ref}(t))$ to determine the value of δ_1. In this case of study, this maximum was derived assuming values for Ω within the range $|\Omega - \Omega_{ref}(t)| = 5 rad/sec$ and the final selection was aided by simulation tests, considering the same disturbances and parameter uncertainties described in section III-A. The chosen values for δ_1, δ_2 and the gains k_1 and k_2 can be found in Appendix *A*.

IV. SIMULATION RESULTS

To assess the designed controllers under realistic conditions, several tests were conducted using a full order model of the WECS including both the mechanical and the electric dynamics, together with uncertainties and disturbances. The fifth order set of differential equations used in these simulations to model the WECS based on DOIG-SKD are detailed in Appendix *C* [27].

The performance of the controlled system is shown herein through a representative example. For the simulations, the system is set to operate in the partial load zone, incorporating disturbances and parameter variations within the ranges summarized in section III-A. The 10-minute wind profile used in the presented simulations can be seen in the upper box of Fig. 5, modeled by adding a high frequency turbulent term to the quasi-steady term, ν_s, which is the one that provides useful work and generates power, and was used for the control design and tracking (see bottom box of Fig. 5) [28]. The bounds of ν_s considered for the design are in Appendix *A*.

A. Variable-Gain Super-Twisting

The evolution of the rotational speed and the reference Ω_{ref} is depicted in Fig. 6. After a brief reaching time the difference between the two variables is negligible, as it can be appreciated

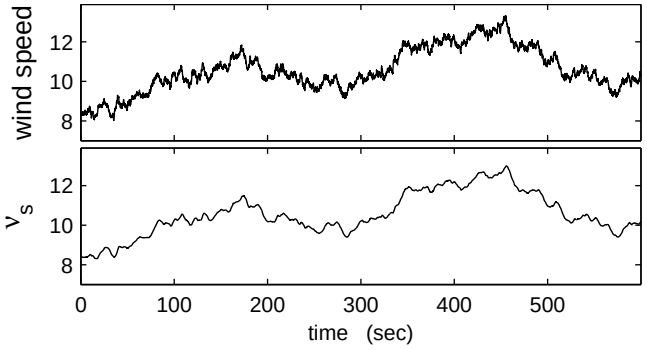

Fig. 5. Wind speed profile and quasi-steady term.

in the zoom box. The sliding variable is presented in Fig. 7, where the practical fulfilment of condition $\sigma = \frac{J}{B_1}(\Omega - \Omega_{ref}(t)) = 0$ can be observed, as well as it can be inferred from the comparison of both speeds curves in Fig. 6. Note that the system operates in sliding exhibiting practically no chattering and proving the robustness of the controller in the presence of the aforementioned disturbances.

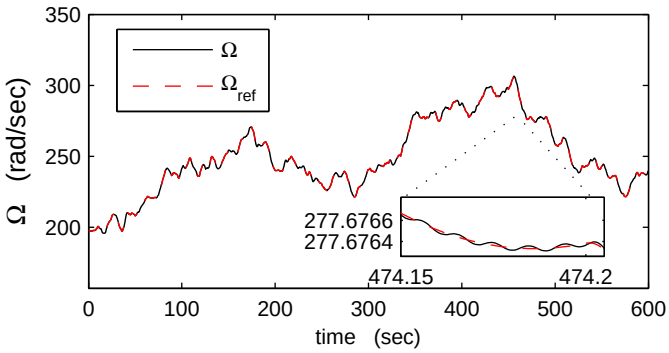

Fig. 6. Rotational speed and speed reference.

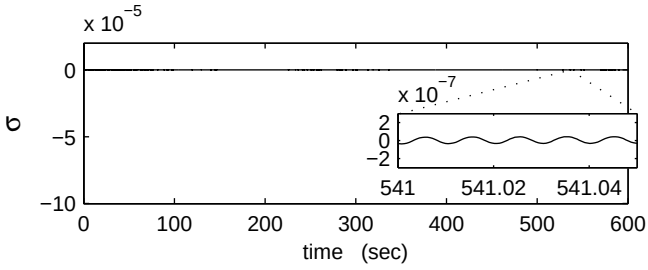

Fig. 7. Sliding variable $\sigma(t)$.

Illustratively, the trajectory of the controlled system in the state space ($\sigma - \dot{\sigma}$ plane) is shown in Fig. 8.

The maximum available power in the wind, i.e. (1) with $\lambda = \lambda_{opt}$ and the generator power are plotted in Fig. 9. As the system successfully operates with $\lambda = \lambda_{opt}$ ($\sigma = 0$), the primary control objective is satisfactorily attained and the generator power finely follows the maximum, except for the gusts and turbulence and an offset due to friction an other losses.

The electrical resistant torque of the generator $-T_e$ and the turbine torque are shown in Fig. 10 together with the

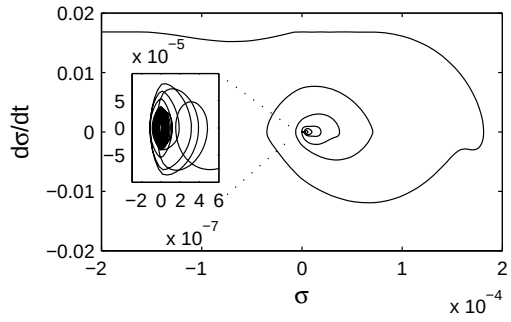

Fig. 8. $\sigma - \dot{\sigma}$ plane.

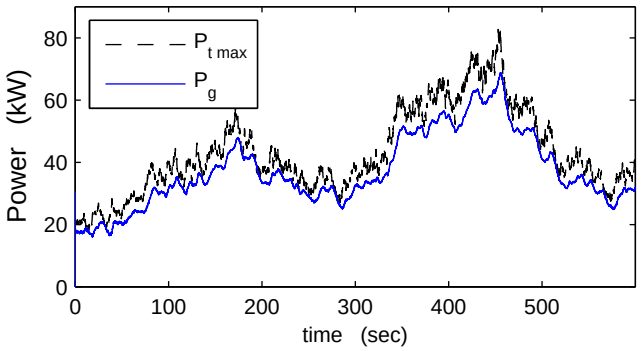

Fig. 9. Maximum available power in the wind and generator power.

unmodeled friction torque T_{fr}. A detail of the generator torque oscillations is shown in the zoomed image inside the figure. The small amplitude of this oscillations can be appreciated, showing the excellent behavior of the controlled system regarding mechanical loads.

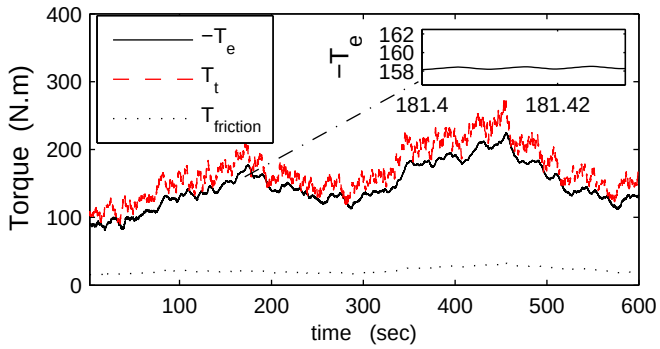

Fig. 10. Generator, turbine and friction torques.

The evolution of the control input, $u(t) = |\cos(\alpha)|$, is depicted in Fig. 11. Note that its smoothness and, therefore, the smoothness of the physical control input α are responsible for the reduced mechanical stresses and practically absence of chattering.

Finally, the electric variables of the WECS are depicted. The $d-q$ components of the stator and rotor currents and voltages can be seen in Fig. 12 and 13 respectively.

B. Fixed-Gain Super-Twisting and comparison

The simulations for the WECS using the fixed-gain controller designed in section III-B demonstrated the achievement

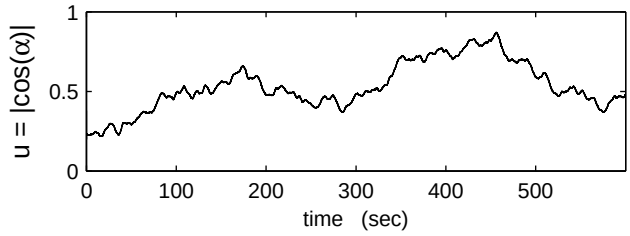

Fig. 11. Control action $u = |\cos(\alpha)|$.

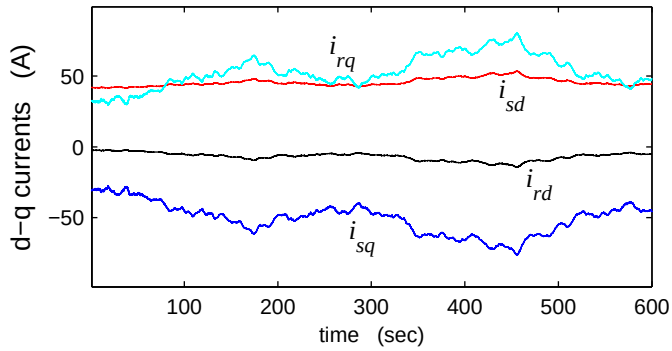

Fig. 12. d-q components of stator and rotor electrical currents.

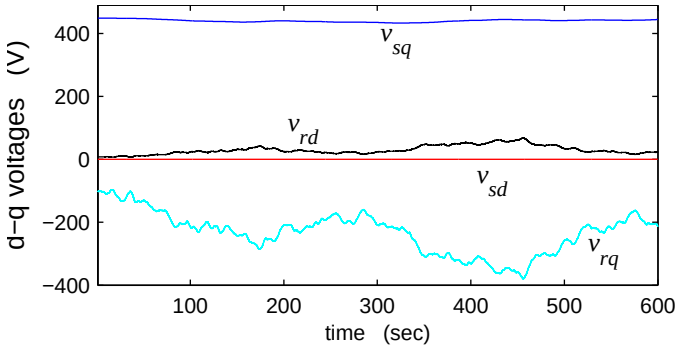

Fig. 13. d-q components of stator and rotor voltages.

of the main control objective of maximizing the captured power. The controller proved its robustness to the several disturbances and uncertainties already described, maintaining the chattering and mechanical stresses at low levels. Representative simulated results, corresponding to the wind profile displayed at the beginning of the section (Fig. 5), are presented and discussed in the sequel, comparing them to the ones corresponding to the variable-gain controller.

The rotational speed and the reference Ω_{ref} are displayed together in Fig. 14. As in the case of the previous controller, the difference between both variables is negligible, consequently fulfilling the sliding condition. The oscillations shown in the zoom boxes of Figs. 6 and 14, which are directly related to the chattering, allows to mention that, although both cases exhibit an excellent tracking behavior in this regard, the variable-gain controller is better.

The time profiles of the electrical and the turbine torques, $-T_e$ and T_t respectively, are depicted in Fig. 15. A look at its zoom box evidences the satisfactory mechanical behavior, existing oscillations which are kept below 4%. The comparison

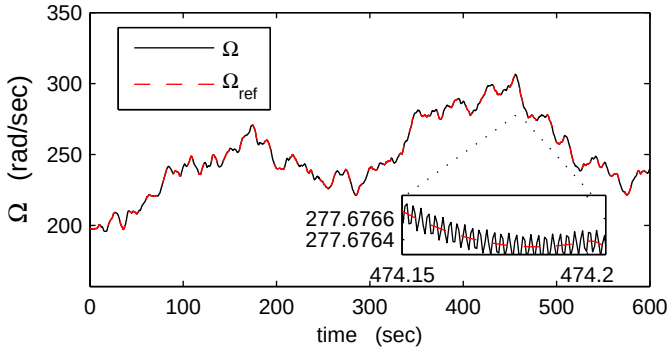

Fig. 14. Rotational speed and speed reference (Fixed-Gain ST).

with the case of the variable-gain controller (see Fig. 10), where the variations of the generator torque are maintained smaller than 0.2%, shows the improvement obtained on this matter by having variable gains in the control action. Note that from the standpoint of mechanical stress, the variations of the torque applied to the shaft is reduced by 20 times in the case of the variable gain design, without significantly increasing the complexity of the control.

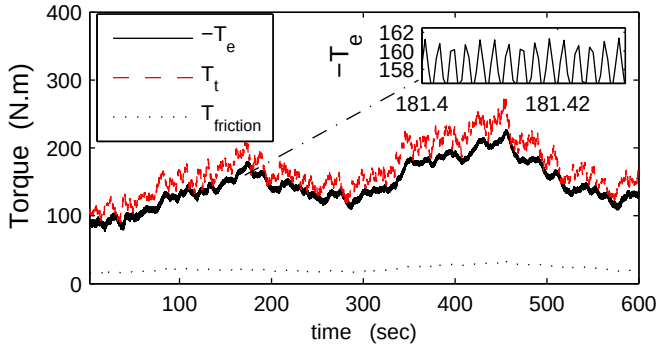

Fig. 15. Generator, turbine and friction torques (Fixed-Gain ST).

Finally, the time evolution of the control input, $u(t) = |\cos(\alpha)|$, is presented in Fig. 16. When compared to the one corresponding to the variable-gain algorithm (Fig. 11), the smoothness of the latter must be pointed out, being it the responsible for the better mechanical behavior.

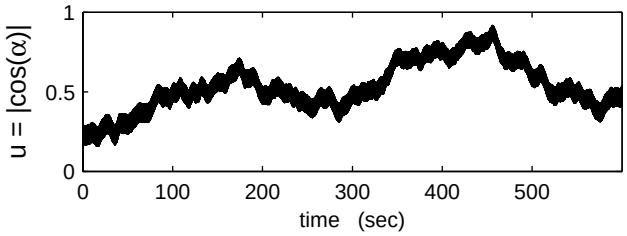

Fig. 16. Control action $u = |\cos(\alpha)|$ (Fixed-Gain ST).

V. CONCLUSIONS

In this paper a super-twisting algorithm with variable gains was applied to the control of a variable-speed WECS with slip power recovery to maximize the energy extracted from the wind. A Lyapunov based controller was designed considering a reduced model of the WECS and tested afterwards through extensive simulations using a realistic full order model, including several disturbances and uncertainties.

The design procedure required the finding of analytical expressions for certain functions to bind such disturbances and uncertainties. Those functions, together with five design parameters, were employed in the calculation of the variable gains of the controller. The find of the bounds and the overall controller tuning is not straightforward, but it is an off-line procedure. On the other hand, the resultant WECS control algorithm is relatively simple, hence the online computational cost is considerably low.

The proposed strategy proved to be suitable for this WECS application, showing a highly robust behavior at accurately tracking the maximum conversion efficiency, which is determined by the randomly varying wind speed. A special important feature of the control law synthesized following this ST approach is the smoothness of the converter firing angle, facilitating its realizability in commutated systems and allowing captured power maximization, very low mechanical stress and practically no output chattering.

An additional controller based on the ST algorithm with fixed gains, also Lyapunov designed, was developed for the studied WECS. Simulations ran under conditions similar to the variable-gain case proved robust tracking behavior. Regarding chattering and mechanical fatigue, the controller has an acceptable performance. However, it must be pointed out the improvement of the variable-gain ST controller in this matter.

VI. ACKNOWLEDGMENTS

This work was supported by UNLP, CONICET and SECyT in Argentina, and by projects PAPIIT 17211 and CONACyT 56819 and 132125 in México.

APPENDIX

A. Nominal and design parameters

$P_{rated} = 60kW$; $\omega_s = 2\pi 50 rad/s$; $V_s = 460/\sqrt{3}$;
$R_s = 119m\Omega$; $R_r = 238m\Omega$; $R_f = 25.9m\Omega$;
$L_s = L_r = 1.4mH$; $L_f = 10.1mH$; $M_s = 35.1mH$;
$\rho = 1.2242 Kg/m^3$; $J = 7.0623 Kgm^2$; $R = 6.75m$;
$c_0 = -1.142\,10^{-2}$; $c_1 = 2.214\,10^{-4}$; $c_2 = -1.03\,10^{-6}$;
$c_3 = 1.191\,10^{-9}$; $n_1 = n_2 = 1.2$; $p_p = 2$;
$A_3 = 8.117$; $A_2 = 3.664$; $A_1 = 7.59$; $A_0 = 0.02$;
$|\ddot{\nu}_s| \leq 0.09$; $|\ddot{\nu}_s| \leq 0.07$; $|\nu_s^{(3)}| \leq 0.01$; $k_c = 0.072$;
$\epsilon = 0.001$; $p_3 = 0.0069$; $p_2 = -0.002$; $p_1 = 0.00579$;
$\delta_1 = 0.62$; $\delta_2 = 0.01$; $k_1 = 130$; $k_2 = 2.37$;
$\delta = 0.0001$;

Rendering to the fast shaft side: $k_{gb} = 19.85$; $T_t = T_{t\text{low}}/k_{gb}$; $\Omega = \Omega_t k_{gb}$; $J = (J_t/k_{gb}^2 + J_g)$, where J_t and J_g are the inertia of the turbine rotor and of the generator rotating parts respectively.

B. Expression for $\tilde{G}(z_1,t)$

$$\tilde{G}(z_1,t) = z_1^3\frac{9n^2\pi R^6 V_s'^3\rho}{2J^3\nu^2R_b^3\Omega_s^2}\Big(V_s'\nu R_b\Delta c_3 - 2c_3V_s'\Delta R_b\,\nu+ + c_3R_b(V_s'\Delta\nu - 4\Delta V_s\,\nu)\Big) + F(z_1,t) - F(0,t)+ + T_{fr}(z_1,t) + z_1^2\frac{3n\pi R^5V_s'\rho}{2J^2R_b^2\Omega_s}\Big(c_2(2\Delta V_s'\,R_b - V_s'\Delta R_b)- - 3V_s'\Delta R_b\,c_3\lambda_{opt} + R_b\Big(3\lambda_{opt}(2\Delta V_s'\,c_3 + V_s'\Delta c_3)+ + V_s'\Delta c_2\Big)\Big) + \frac{z_1}{2JR_b^2\Omega_s^2}\Big(6V_s'^2\Delta R_b - 12V_s'\Delta V_s'\,R_b+ + \pi R^4\rho R_b^2\Omega_s^2\Big(\Delta\nu\,c_1 + \nu\Delta c_1 + \lambda_{opt}(2\Delta\nu\,c_2 + 2\nu\Delta c_2)+ + 3\lambda_{opt}^2(\Delta\nu\,c_3 + \nu\Delta c_3)\Big)\Big) - \lambda_{opt}\frac{3V_s'^2\Delta\nu + J\Delta R_b\Omega_s^2\dot{\nu}}{3nRV_s'^2\Omega_s}+ + \frac{\pi R^3\nu\rho\Omega_s}{6nV_s'^3}\sum_{i=0}^{3}\Big(\big(V_s'\Delta R_b\,\nu + 2R_b(V_s'\Delta\nu - \nu\Delta V_s')\big)c_i+ + V_s'\nu R_b\Delta c_i\Big)\lambda_{opt}^i + \frac{\lambda_{opt}R_bJ\Omega_s}{3nRV_s'}(2\Delta V_s'\dot{\nu} - V_s'\Delta\nu\,\ddot{\nu})$$

C. Park model

The nonlinear differential equations that describe the topology under study in a synchronously rotating direct quadrature (d-q) frame are

$$\begin{bmatrix} 0 \\ V_s \\ -(V_s'')'u\sin(\varphi) \\ -(V_s'')'u\cos(\varphi) \end{bmatrix} = \mathbf{Z}\begin{bmatrix} i_{sd} \\ i_{sq} \\ i'_{rd} \\ i'_{rq} \end{bmatrix}\quad , \tag{40}$$

with

$$\mathbf{Z} = \begin{bmatrix} R_s + L_sp & -w_sL_s & M_sp & -\omega_sM_s \\ \omega_sL_s & R_s + L_sp & \omega_sM_s & M_sp \\ M_sp & -s\omega_sM_s & R'_b + L'_bp & -s\omega_sL'_r \\ s\omega_sM_s & M_sp & s\omega_sL'_r & R'_b + L'_bp \end{bmatrix}$$

where p is the time derivative operator, $\varphi = \tan^{-1}\left(\frac{i_{rd}}{i_{rq}}\right)$, $L_b = L_r + 0.55L_f$, with L_r and L_f the inductances of rotor and dc-link, respectively, and M_s the magnetizing inductance. Quotation marks applied to V_s indicates it has been referred to the inverter terminals by n_2. The equation for the generator torque, which replaces (5), is

$$T_e = p_pM_s(i_{sq}i'_{rd} - i_{sd}i'_{rq}) \tag{41}$$

where p_p corresponds to the number of pole pairs.

REFERENCES

[1] "Global wind energy output 2010," Global Wind Energy Council, Tech. Rep., Oct. 2011. [Online]. Available: http://www.gwec.net

[2] "World wind energy report 2010," World Wind Energy Association, Tech. Rep., Apr. 2011. [Online]. Available: http://www.wwindea.org/

[3] B. Beltran, T. Ahmed-Ali, and M. Benbouzid, "High-order sliding-mode control of variable-speed wind turbines," *IEEE Trans. Ind. Electron.*, vol. 56, no. 9, pp. 3314 –3321, Sep. 2009.

[4] G. Bartolini, A. Ferrara, and E. Usai, "Chattering avoidance by second order sliding mode control," *IEEE Trans. Autom. Control*, vol. 43, no. 2, pp. 241–246, 1998.

[5] G. Bartolini, A. Levant, A. Pisano, and E. Usai, "2-sliding mode with adaptation," in *Procs. 7th IEEE Mediterranean Conference on Control and Systems*, Haifa, Israel, 1999.

[6] I. Boiko, L. Fridman, A. Pisano, and E. Usai, "Analysis of chattering in systems with second-order sliding modes," *IEEE Trans. Autom. Control*, vol. 52, no. 11, pp. 2085–2102, Nov. 2007.

[7] C. Edwards, E. Fossas Colet, and L. Fridman, Eds., *Advances in Variable Structure and Sliding Mode Control*. Berlin: Springer, 2006.

[8] S. Emelyanov, S. Korovin, and A. Levant, "High-order sliding modes in control systems," *Computational Mathematics and Modeling*, vol. 7, no. 3, pp. 294–318, 1996.

[9] L. Fridman and A. Levant, *Sliding Mode Control in Engineering*. Marcel Dekker, Inc., 2002, ch. 3, pp. 53–101.

[10] J. Hung, W. Gao, and J. Hung, "Variable structure control: a survey," *IEEE Trans. Ind. Electron.*, vol. 40, no. 1, pp. 2–22, 1993.

[11] A. Levant, "Sliding order and sliding accuracy in sliding mode control," *International Journal of Control*, vol. 58, no. 6, pp. 1247–1263, 1993.

[12] ——, "Principles of 2-sliding mode design," *Automatica*, vol. 43, no. 4, pp. 576–586, April 2007.

[13] A. Sabanovic, L. M. Fridman, and S. Spurgeon, Eds., *Variable Structure Systems: From Principles to Implementation*. IET, UK, 2004.

[14] H. Shi, Y. Feng, and X. Yu, "High-order terminal sliding modes control for induction motor," in *IECON 2010 - 36th Annual Conference on IEEE Industrial Electronics Society*, Nov. 2010, pp. 2391–2395.

[15] Q. Ahmed and A. Bhatti, "Estimating si engine efficiencies and parameters in second-order sliding modes," *IEEE Trans. Ind. Electron.*, vol. 58, no. 10, pp. 4837–4846, Oct. 2011.

[16] S. Benelghali, M. El Hachemi Benbouzid, J. Charpentier, T. Ahmed-Ali, and I. Munteanu, "Experimental validation of a marine current turbine simulator: Application to a permanent magnet synchronous generator-based system second-order sliding mode control," *IEEE Trans. Ind. Electron.*, vol. 58, no. 1, pp. 118–126, Jan. 2011.

[17] A. Dávila, J. Moreno, and L. Fridman, "Variable gains super-twisting algorithm: A Lyapunov based design," in *Procs. 2010 American Control Conference*, Baltimore, MD, USA, Jun. 2010.

[18] J. A. Moreno and M. Osorio, "A lyapunov approach to second-order sliding mode controllers and observers," in *Procs. 47th IEEE Conference on Decision and Control, CDC 2008*, Dec. 2008, pp. 2856–2861.

[19] J. Baroudi, V. Dinavahi, and A. Knight, "A review of power converter topologies for wind generators," *Renewable Energy*, vol. 32, no. 14, pp. 2369–2385, Nov. 2007.

[20] Z. Salameh and L. Kazda, "Analysis of the steady state performance of the double output induction generator," *IEEE Trans. Energy Convers.*, vol. 1, no. 1, pp. 26–32, 1986.

[21] R. Spée, S. Bhowmik, and J. Enslin, "Novel control strategies for variable-speed doubly fed power generation systems," *Renewable Energy*, vol. 6, no. 8, pp. 907–915, Nov. 1995.

[22] I. Munteanu, S. Bacha, A. Bratcu, J. Guiraud, and D. Roye, "Energy-reliability optimization of wind energy conversion systems by sliding mode control," *IEEE Trans. Energy Convers.*, vol. 23, no. 3, pp. 975–985, Sep. 2008.

[23] T. Burton, D. Sharpe, N. Jenkins, and E. Bossanyi, *Wind Energy handbook*. England: John Wiley and Sons, 2001.

[24] H. De Battista, P. Puleston, R. Mantz, and C. Christiansen, "Sliding mode control of wind energy systems with doig–power efficiency and torsional dynamics optimization," *IEEE Trans. Power Syst.*, vol. 15, no. 2, pp. 728–734, May 2000.

[25] V. Utkin, "Sliding mode control design principles and applications to electric drives," *IEEE Trans. Ind. Electron.*, vol. 40, no. 1, pp. 23–36, 1993.

[26] H. Khalil, *Nonlinear Systems*, 3rd ed. Upsaddle River, New Jersey: Prentice-Hall, 2002.

[27] P. Puleston, R. Mantz, P. Battaiotto, and F. Valenciaga, "Sliding mode control for efficiency optimization of wind energy systems with double output induction generator," *Int. J. Energy Research*, vol. 24, no. 1, pp. 77–92, 2000.

[28] F. D. Bianchi, H. de Battista, and R. Mantz, *Wind Turbine Control Systems: Principles, Modeling and Gain Scheduling Design*. London: Springer, 2007.